Parameter Identification and Lyapunov Function Based Adaptive Switched Control for Underwater Electroacoustic Transduction System

Xinwei Wei, Hongliang Wang, *Senior Member, IEEE*, An Luo, *Senior Member, IEEE*, Fujun Ma, *Member, IEEE*, Zhen Zhu, Gaoxiang Li, and Renyifan Hao

***Abstract*—The underwater electroacoustic transduction system is widely used in underwater navigation, ranging, and communication. However, it is difficult to control the current of the giant magnetostrictive transducer (GMT) for a voltage mode amplifier, because nonsinusoidal waves without constant fundamental frequencies may be required, and the load parameters of the GMT vary greatly with its working frequency, current, and condition. A parameter online identification algorithm is proposed for the GMT, where only one matrix inversion and one filtering for a two-dimensional matrix are required. A discretized switched control is derived, which selects the subsystem minimizing the Lyapunov function of tracking error in each control period. In addition, a switching state selection method making the switching frequencies lower and consistent is also used to cooperate with the switched control. Finally, the adaptive switched control is experimentally verified on the designed 1-kW electroacoustic transduction platform.**

***Index Terms*—Acoustic transducers, adaptive control, parameter estimation, power amplifier, switching frequency.**

I. Introduction

CONSISTING of a digital power amplifier and an underwater electroacoustic transducer, the underwater electroacoustic transduction system (UETS) is widely used for ocean acoustic tomography, long-range navigation, geophysical seismic bottom imaging, continuous active sonar, and long-range communications [1]–[3]. There have been several successful cases in the past two decades, such as Pacific Ocean, Pioneer Seamount (2001); MOVE Experiment (2004–2005); Pacific Ocean, Hoke Seamount (2002–2004); NPAL04, SPICE04, Pacific Ocean (2004–2005); Fram Strait 2008-2016; Philippine Sea (2009, 2010–2011); Newfoundland, Canada (2014–2015), Arctic (2016–2017) [4]–[6]. The existing UETSs have shown excellent performance in these cases, but years of operating experience still show that the existing technology needs to be improved and developed. Many applications demand a sound source with constant parameters and a wide frequency response with small amplitude variability for an arbitrary waveform radiation [4], [5].

One possible method to achieve this goal is precisely closed-loop control of the voltage or current of the transducer, which is the equipment that generates the sound source [7], [8]. But, the closed-loop control of the giant magnetostrictive transducer (GMT) is a very complex but meaningful issue [9]. This is due to the following reasons. First, the GMT is a current-driven load, but the commonly used digital power amplifiers are usually voltage based, composing of voltage-source inverters and *LC* filters. Second, as a resistive-inductive load, the equivalent inductance and resistance of the GMT vary greatly with its working frequency, current, and conditions [9]–[11]. Some undesirable results may occur, such as control error, waveform distortion, or even overcurrent, if the significant parameter variations are ignored [9]. In addition, the system stability and transient response will also be affected [12]. Third, the output waveform can be an arbitrary waveform, not necessarily a sine wave, such as a chirp signal [6]. This also requires the current closed-loop controller to have a very fast dynamic performance, and the control methods in *dq* rotating coordinate frame adopted by flexible ac transmission systems and ac motor drive will be not suitable for the UETS [13]–[15].

Aiming at the closed-loop control problem of digital power amplifiers, a single closed-loop PI controller was used for cascaded *H*-bridge digital power amplifiers in [16]. However, the gain of a PI controller decreased with the increase of the output frequency, and it was difficult to achieve system stability and high precision tracking of a given arbitrary waveform simultaneously. In [17], a dual closed-loop PI control for multilevel digital amplifiers was designed, and the bandwidth was increased compared with the single closed-loop controller in [16]. But, the controller was designed for a resistive load with constant value. Its robustness might greatly decrease with the variations of the load characteristics or parameters. In [18], the digital one-cycle control technology was used for current-mode digital power amplifiers, which improved the control accuracy and reduced the current ripple. In [19] and [20], sliding mode controllers were applied to voltage mode digital power amplifiers. In [21], the

Manuscript received February 25, 2019; revised August 12, 2019; accepted October 30, 2019. Date of publication November 11, 2019; date of current version February 20, 2020. This work was supported by the National Natural Science Foundation of China under Grants 51837005 and 51977069. Recommended for publication by Associate Editor B. Semail. *(Corresponding author: Hongliang Wang.)*

The authors are with the College of Electrical and Information Engineering, Hunan University, Changsha 410082, China (e-mail: 18774880723@163.com; liangliang-930@163.com; an_luo@hnu.edu.cn; mafujun2004@163.com; 332120507@qq.com; 1511872579@qq.com; 530187735@qq.com).

Color versions of one or more of the figures in this article are available online at http://ieeexplore.ieee.org.

Digital Object Identifier 10.1109/TPEL.2019.2953138

phase lead was adaptively compensated based on unsymmetrical current sampling resistance network. In [22], the dead beat control method was used for current control in cascaded *H*-bridge converters. However, control methods in [18]–[22] worked on the basis of pulsewidth modulation (PWM), so good control effect appeared only when the switching frequency was high enough. Since the power amplifier topology studied in this article is a full-bridge neutral-point-clamped (NPC) inverter, the control methods of this topology is also investigated here. In [23], model predictive control (MPC), which could ensure fixed frequency of power switches was applied to full-bridge NPC converters. However, the dynamic performance of the MPC would decrease with fixed switching frequency. In [24], the MPC, which could reduce switching frequencies was applied to a single phase uninterruptible power supply (UPS) using the full-bridge NPC inverter topology. However, the switching state selection method was added in the cost function. Thus, the more complicated cost function needed to be calculated nine times, which required more computation, and the consistency of switching frequencies could not be achieved.

Aiming at the variable characteristics of the equivalent inductance and resistance of the GMT, the load parameters are intended to be identified online in this article, which will improve control accuracy and system robustness. On parameter identification and estimation, in [25], the iteration least square method was proposed for parameter estimation of dc– converters. In [26]–[28], the inductance of control objectives were measured or estimated online/offline. In [29] and [30], load observer was used to estimate load parameters online of motor drives and UPSs. However, the algorithms in [25]–[30] cost large amount of computing resources. In [31]–[33], multiple methods were used in grid-tied inverters to identify the impedance of the grid. However, these methods were designed for sine wave systems with limited frequency range of 50 $\pm$ 0.5 or 60 $\pm$ 0.5 Hz. The special situation that nonsinusoidal waves without constant fundamental frequencies were required in the UETS was not considered.

In this article, an efficient and simple load parameter online identification algorithm (POIA) is proposed, which is favorable to realize adaptive control and greatly improves the robustness of the closed-loop controller. After that, a discretized switched control based on Lyapunov function (DSCBOLF) for UETS is derived, which can achieve high precision tracking of the current of the GMT, and make the switching frequencies lower and consistent, at the expense of little computation.

The rest of this article is organized as follows. In Section II, the POIA considering the equivalent parameter variations is proposed for the GMT. In Section II, the studied UETS is built as a switched system model. In Section III, a DSCBOLF is derived, and a novel switching state selection method is also proposed to cooperate with the DSCBOLF. Section V reports the experiment results and Section VI gives the conclusion of this article.

II. Basic Principle and Parameter Online Identification of Magnetostrictive Transducers

The structure of a typical UETS is shown in Fig. 1. The main circuit topology of the digital power amplifier studied in this

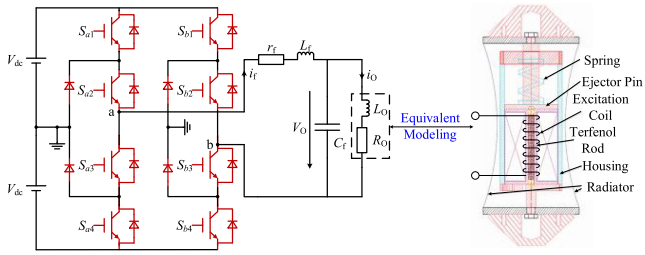

Fig. 1. UETS using the full-bridge NPC inverter and the GMT.

TABLE I
Actual Parameters of the Studied UETS

Parameter	Value
DC bus voltage V_{dc}	75 V
Filter inductance L_f	2 mH
Filter inductance parasitic resistance r_f	0.14 Ω
Filter capacitance C_f	4.7 μF
Output frequency band	100 Hz–1000 Hz
Rated current of the GMT	3 A

article is a full-bridge NPC inverter with an *LC* filter, which features lower voltage stress on power semiconductors, lower voltage harmonics, and smaller electromagnetic interference, and is widely used in medium and high power applications.

The dc input of the amplifier is provided by two dc voltage sources. In the full-bridge NPC inverter, S_{xi} for all $i \in \{1, \ldots, 4\}$ and $x \in \{a, b\}$ denotes the switching signal to trigger each power switch. Besides, L_f denotes the filter inductor, r_f denotes the parasitic resistor of L_f, i_f denotes the current of L_f. C_f denotes the filter capacitor, V_O denotes the voltage of C_f, and i_O denotes the current of the GMT. The load of the UETS is a GMT, which is equivalently modeled as a resistive–inductive load with parameters of L_O and R_O [34]. The actual parameters of the studied UETS is given in Table I.

A. Basic Principle of Giant Magnetostrictive Transducers

A transducer refers to the device that can realize the mutual conversion of electric energy and sound energy, including the transmitter that sends sound signal and the hydrophone that receives sound signal. In this article, it specifically refers to the transmitter that transduces electric energy into sound energy to realize an arbitrary waveform transmission. At present, the commonly used transducers in the field of underwater acoustic include two types, the piezoelectric ceramic ones and the giant magnetostrictive ones. Because of the remarkable high energy density and large deformation coefficient of Terfenol-D, the magnetostrictive material, GMTs are widely used in various types of low-frequency and high power underwater acoustic sources, exploration sonar systems, and underwater remote communication fields [35]–[37].

The right side of Fig. 1 shows the structure of a flexural type GMT. The alternating magnetic field in the Terfenol rod is established by the excitation coil that flows through an alternating current. Therefore, the Terfenol rod will elongate or shorten in the alternating magnetic field, so that the mechanical vibration

is generated and the sound is radiated [34]. In general, the GMT operates at a low frequency range for underwater communication and navigation systems. In this case, the GMT can be regarded as a resistive–inductive load. In the GMT, an excitation coil with many turns is used to establish alternating magnetic field in the Terfenol rod, which composes the inductive part of the load, and the resistive part is composed of the static resistance, the eddy current loss, the hysteresis loss, and the sound resistance reflecting the power consumption for sound radiations [9]–[11], [34]. As a current driven instrument, the driving current of the GMT is better to be closed-loop controlled. However, the closed-loop control is difficult to be achieved because of the significant variations of the equivalent parameters [9]–[11].

The equivalent parameters of the GMT vary with its working frequency mainly due to the different skin effects at different frequencies [38]. They also change with the working current, because the hysteresis may lead to several nonlinear phenomena, such as saturation [10]. Moreover, the variations are also related to the working condition where various disturbance factors exist, such as the water density, depth, and temperature [11]. The used GMT in this article is taken as an example to show the changing range of these parameters. At 100 Hz, the identified resistance is 8.9 Ω, and the identified inductance is 10 mH, while they change to 16.5 Ω and 4.39 mH respectively at 1000 Hz. It can be seen that the identified resistance increases by 85%, and the identified inductance decreases by 56%. Thus, some undesirable results may occur, such as control error, waveform distortion, or even overcurrent, if we ignore the significant parameter variations [9]. In addition, the system stability and transient response will also be affected [12]. Although the equivalent impedance is usually measured by an impedance measurement instrument before designing the control method, they are not equal to the actual equivalent impedances under normal operation. Therefore, the online identification of parameter variations is of great significance to realize the real-time current tracking of the GMT with strong robustness in a wide bandwidth.

B. Parameter Online Identification Algorithm

In this article, a novel POIA is proposed for the parameter variations of the GMT. According to Fig. 1, the terminal voltage of the GMT $V_{\rm O}$, the current of the GMT $i_{\rm O}$, and the equivalent inductance $L_{\rm O}$ and resistance $R_{\rm O}$ satisfy the following:

$$V_{\rm O} = L_{\rm O}\frac{di_{\rm O}}{dt} + R_{\rm O}i_{\rm O}. \tag{1}$$

The equivalent parameters $R_{\rm O}$ and $L_{\rm O}$ can be assumed as constant during two consecutive identification periods due to their relatively slow rate of change, then (1) can be discretized using the *implicit trapezoidal integral method* as (2)

$$\begin{cases} \frac{V_{\rm O}(n)+V_{\rm O}(n-1)}{2} = L_{\rm O}\frac{i_{\rm O}(n)-i_{\rm O}(n-1)}{T_{\rm D}} + R_{\rm O}\frac{i_{\rm O}(n)+i_{\rm O}(n-1)}{2} \\ \frac{V_{\rm O}(n-1)+V_{\rm O}(n-2)}{2} = L_{\rm O}\frac{i_{\rm O}(n-1)-i_{\rm O}(n-2)}{T_{\rm D}} \\ \qquad\qquad + R_{\rm O}\frac{i_{\rm O}(n-1)+i_{\rm O}(n-2)}{2} \end{cases} \tag{2}$$

where $T_{\rm D}$ denotes the identification period. $V_{\rm O}(n-2)$, $V_{\rm O}(n-1)$, and $V_{\rm O}(n)$ denote the true values of $V_{\rm O}$ at $(n-2)T_{\rm D}$, $(n-1)T_{\rm D}$ and $nT_{\rm D}$ instant, respectively. Similarly, $i_{\rm O}(n-2)$, $i_{\rm O}(n-1)$, and $i_{\rm O}(n)$ denote the true values of $i_{\rm O}$ at $(n-2)T_{\rm D}$, $(n-1)T_{\rm D}$, and $nT_{\rm D}$ instant, respectively.

In order to distinguish the true values from the sampling values, the sampling values of $V_{\rm O}$ and $i_{\rm O}$ are denoted in the form of $\hat{(\cdot)}$. As we all know, the sampling values can be obtained by signal sensors and sampling chips, where certain amounts of measurement noises always exist. Therefore, the identification results based on the sampling values can be regarded as the preliminary result, which can be calculated by (3), and denoted by $L_{\rm Op}(n)$ and $R_{\rm Op}(n)$

$$\begin{aligned} &\begin{bmatrix} L_{\rm Op}(n) \\ R_{\rm Op}(n) \end{bmatrix} \\ &= \begin{bmatrix} \frac{\hat{i}_{\rm O}(n)-\hat{i}_{\rm O}(n-1)}{T_{\rm D}} & \frac{\hat{i}_{\rm O}(n)+\hat{i}_{\rm O}(n-1)}{2} \\ \frac{\hat{i}_{\rm O}(n-1)-\hat{i}_{\rm O}(n-2)}{T_{\rm D}} & \frac{\hat{i}_{\rm O}(n-1)+\hat{i}_{\rm O}(n-2)}{2} \end{bmatrix}^{-1} \\ &\quad\times \begin{bmatrix} \frac{\hat{V}_{\rm O}(n)+\hat{V}_{\rm O}(n-1)}{2} \\ \frac{\hat{V}_{\rm O}(n-1)+\hat{V}_{\rm O}(n-2)}{2} \end{bmatrix}. \end{aligned} \tag{3}$$

In order to reduce the influence of measurement noise on the preliminary results, first-order low-pass filters can be used to improve the calculation results of (3). Therefore, the final identification results, denoted by $L_{\rm O}(n)$ and $R_{\rm O}(n)$, can be obtained, respectively, as follows:

$$L_{\rm O}(n) = aL_{\rm Op}(n) + (1-a)L_{\rm O}(n-1) \tag{4}$$

$$R_{\rm O}(n) = aR_{\rm Op}(n) + (1-a)R_{\rm O}(n-1) \tag{5}$$

where $a = 2\pi fT_{\rm D}/(1+2\pi fT_{\rm D})$, and f denotes the cutoff frequency of the used first-order low-pass filter.

It can be seen that two difference equations are derived from the differential equation of the GMT only, which allows the proposed POIA to maintain validity even if nonsinusoidal waves without constant fundamental frequencies are required in the UETS. In addition, the proposed POIA only needs one matrix inversion and one filtering for a two-dimensional (2-D) matrix, which allows many calculations and running memory to be saved.

III. Switched System Model of UETS

The output voltage of the full-bridge NPC inverter is denoted by $V_{\rm ab}$. Since the full-bridge NPC inverter can output five levels of 2, 1, 0, −1, and −2, there are five options for $V_{\rm ab}$ to choose from: $2V_{\rm dc}$, $V_{\rm dc}$, 0, $-V_{\rm dc}$, and $-2V_{\rm dc}$. According to Kirchhoff's laws of voltage and current, there are five groups of differential equations that corresponds to the five options, as shown in the

TABLE II
EFFECTIVE SWITCHING STATES

Output Level	Corresponding Switching State
$2V_{dc}$	S1=[1 1 0 0 0 0 1 1]
V_{dc}	S2=[1 1 0 0 0 1 1 0]
	S3=[0 1 1 0 0 0 1 1]
0	S4=[1 1 0 0 1 1 0 0]
	S5=[0 1 1 0 0 1 1 0]
	S6=[0 0 1 1 0 0 1 1]
$-V_{dc}$	S7=[0 1 1 0 1 1 0 0]
	S8=[0 0 1 1 0 1 1 0]
$-2V_{dc}$	S9=[0 0 1 1 1 1 0 0]

following:

$$\begin{cases} L_{\mathrm{f}}\frac{\mathrm{d}i_{\mathrm{f}}}{\mathrm{d}t} = (3-i)\,V_{\mathrm{dc}} - V_{\mathrm{O}} - i_{\mathrm{f}}r_{\mathrm{f}} \\ C_{\mathrm{f}}\frac{\mathrm{d}V_{\mathrm{O}}}{\mathrm{d}t} = i_{\mathrm{f}} - i_{\mathrm{O}} \qquad\qquad ,i \in K=\{1,2,3,4,5\} \\ L_{\mathrm{O}}\frac{\mathrm{d}i_{\mathrm{O}}}{\mathrm{d}t} = V_{\mathrm{O}} - R_{\mathrm{O}}i_{\mathrm{O}} \end{cases} \tag{6}$$

where i denotes the number of the option, K denotes the set of the option numbers. If the ith option is selected, V_{ab} is equal to $(3-i)V_{\mathrm{dc}}$.

Selecting i_{f}, V_{O}, and i_{O} as the state variables of the system, (7) can be obtained from (6) as

$$\begin{bmatrix} \dot{i}_{\mathrm{f}} \\ \dot{V}_{\mathrm{O}} \\ \dot{i}_{\mathrm{O}} \end{bmatrix} = \begin{bmatrix} -\frac{r_{\mathrm{f}}}{L_{\mathrm{f}}} & -\frac{1}{L_{\mathrm{f}}} & 0 \\ \frac{1}{C_{\mathrm{f}}} & 0 & -\frac{1}{C_{\mathrm{f}}} \\ 0 & \frac{1}{L_{\mathrm{O}}} & -\frac{R_{\mathrm{O}}}{L_{\mathrm{O}}} \end{bmatrix} \begin{bmatrix} i_{\mathrm{f}} \\ V_{\mathrm{O}} \\ i_{\mathrm{O}} \end{bmatrix} + \begin{bmatrix} \frac{V_{\mathrm{dc}}}{L_{\mathrm{f}}} \\ 0 \\ 0 \end{bmatrix} (3-i), i \in K = \{1,2,3,4,5\}. \tag{7}$$

The array $S = [S_{a1}\ S_{a2}\ S_{a3}\ S_{a4}\ S_{b1}\ S_{b2}\ S_{b3}\ S_{b4}]$ is defined to denote the switching state of the eight power switches in the full-bridge NPC inverter. In the normal operation, there are nine effective switching states as given in Table II.

The state variable array can be denoted by $x = [i_{\mathrm{f}}\ V_{\mathrm{O}}\ i_{\mathrm{O}}]^{\mathrm{T}}$, and A and B are also defined, respectively, as follows:

$$A = \begin{bmatrix} -\frac{r_{\mathrm{f}}}{L_{\mathrm{f}}} & -\frac{1}{L_{\mathrm{f}}} & 0 \\ \frac{1}{C_{\mathrm{f}}} & 0 & -\frac{1}{C_{\mathrm{f}}} \\ 0 & \frac{1}{L_{\mathrm{O}}} & -\frac{R_{\mathrm{O}}}{L_{\mathrm{O}}} \end{bmatrix}$$

$$B = \begin{bmatrix} \frac{V_{\mathrm{dc}}}{L_{\mathrm{f}}} \\ 0 \\ 0 \end{bmatrix}.$$

Therefore, the UETS can be modeled as a switched system model with five subsystems in the following:

$$\dot{x} = A_\sigma x + B_\sigma, \sigma \in K. \tag{8}$$

The five subsystems can be listed as follows.

Subsystem 1: $\sigma = 1, A_1 = A, B_1 = 2B, S =$ S1.
Subsystem 2: $\sigma = 2, A_2 = A, B_2 = B, S =$ S2 or S3.
Subsystem 3: $\sigma = 3, A_3 = A, B_3 = 0, S =$ S4 or S5 or S6.
Subsystem 4: $\sigma = 4, A_4 = A, B_4 = -B, S =$ S7 or S8.
Subsystem 5: $\sigma = 5, A_5 = A, B_5 = -2B, S =$ S9.

Furthermore, $x_{\mathrm{ref}} = [i_{\mathrm{fref}}\ V_{\mathrm{Oref}}\ i_{\mathrm{Oref}}]^{\mathrm{T}}$ is used to denote the reference of x. Thus, the tracking error can be expressed by $\xi = x - x_{\mathrm{ref}}$. Then, the affine switched system model reflecting the error dynamic can be expressed by the following:

$$\begin{cases} \dot{\xi} = A_\sigma \xi + b_\sigma \\ b_\sigma = B_\sigma + A_\sigma x_{\mathrm{ref}}. \end{cases}, \sigma \in K \tag{9}$$

IV. SWITCHED CONTROL OF UETS BASED ON LYAPUNOV FUNCTION

A. Switched Control Based on Lyapunov Function

In order to ensure reliable distance measurement and communication of the UETS, stability is the premise of closed-loop control of the current of the GMT. The switched control proposed in [39] could make all the state variables converge to their references as quickly as possible while ensuring the system global stability, which is very suitable for the UETS. It can be expressed as the following theorem.

Theorem 1: For the affine switched system expressed in (9), if there exist a positive definite matrix $P \in R^{n\times n}$ and $\lambda \in K$, such that

$$A_i{}^{\mathrm{T}}P + PA_i + Q_i < 0 \tag{10}$$

$$A_\lambda x_{\mathrm{ref}} + B_\lambda = 0 \tag{11}$$

then, the switching rule in the following:

$$\begin{aligned} \sigma(x) &= \arg\min_{i\in K} \dot{V}_i(\xi) \\ &= \arg\min_{i\in K} \xi^T P(A_i x_{\mathrm{ref}} + B_i) \end{aligned} \tag{12}$$

makes the system globally asymptotically stable at the equilibrium point, x_{ref}. In (11), A_λ and B_λ denote the convex combinations of A_i and B_i, respectively. In (12), $V(\xi) = \xi^{\mathrm{T}}P\xi$ denotes the of the common quadratic Lyapunov function of the affine switched system, and $\dot{V}_i(\xi)$ denotes the derivative of $V(\xi)$ if Subsystem i is selected.

However, there are following problems when the switched rule described in Theorem 1 is applied to power electronic systems with digital controllers. First, in Theorem 1, the switching frequencies are required to be infinitely high. But, that of actual power switches are limited. Second, the controllers are required to calculate P instantaneously by solving the Lyapunov equation $(A_i{}^{\mathrm{T}}P + PA_i + Q_i = 0)$ online from A_i and a given matrix Q_i [40]. As we all know, this is unachievable for actual digital controllers. Third, calculating and sorting the derivatives

of the Lyapunov functions for all subsystems further increases the computational burden.

B. Proposed DSCBOLF for UETS

The work presented in [41] and [42] pointed out that an actual power electronic converter could be regarded as a Hamiltonian system, which allowed the energy function to be used as a Lyapunov function for passive control, if A_i was a Hurwitz matrix. Therefore, in order to avoid solving Lyapunov equation online, a given matrix $P = \mathrm{diag}\{L_\mathrm{f}, C_\mathrm{f}, L_\mathrm{O}\}$ is used to reduce the computational burden greatly. At the same time, the switched rule in (12) is discretized, so that in each control period it runs only once, and the switching state changes up to once. This not only further reduces the computation, but also lowers the required switching frequencies to an acceptable level.

The control period can be denoted by T. Since T is small enough, the switched rule in (12) can be discretized as follows:

$$\begin{aligned}\sigma(t) &= \arg\min_{i\in K}\left\{\dot{V}_i(\xi)\right\}\\ &\approx \arg\min_{i\in K}\left\{\frac{V_i(\xi(k+1),(k+1)T)-V_i(\xi(k),kT)}{T}\right\}\end{aligned} \tag{13}$$

where $V_i(\xi(k+1),(k+1)T)$ and $V_i(\xi(k),kT)$, respectively, denote the values of $V(\xi)$ at $(k+1)T$ and kT instant if Subsystem i is selected. Since $V_i(\xi(k),kT)$ is constant for all subsystems in the $(k+1)$th control period, the choice of $\sigma(t)$ will not be affected. Then, (13) can be simplified as follows:

$$\sigma(t) = \arg\min_{i\in K}\{V_i(\xi(k+1),(k+1)T)\}. \tag{14}$$

In addition, $x_i(k+1)$ can be used to denote the value of x at $(k+1)T$ instant if Subsystem i is selected, and $x_\mathrm{ref}(k+1)$ denotes the value of x_ref at $(k+1)T$ instant. Then, (14) can be further derived as follows:

$$\begin{aligned}\sigma(t) &= \arg\min_{i\in K}\{V_i(\xi(k+1),(k+1)T)\}\\ &= \arg\min_{i\in K}\{(x_i(k+1)-x_{ref}(k+1))^\mathrm{T}\\ &\quad\times P(x_i(k+1)-x_{ref}(k+1))\}\\ &= \arg\min_{i\in K}\{L_\mathrm{f}(i_{\mathrm{f}i}(k+1)\\ &\quad - i_{\mathrm{fref}}(k+1))^2 + C_\mathrm{f}(V_{\mathrm{O}i}(k+1)\\ &\quad - V_{\mathrm{Oref}}(k+1))^2 + L_\mathrm{O}(i_{\mathrm{O}i}(k+1)-i_{\mathrm{Oref}}(k+1))^2\}.\end{aligned} \tag{15}$$

In order to obtain $x_i(k+1) = [i_{\mathrm{f}i}(k+1)V_{\mathrm{O}i}(k+1)\ i_{\mathrm{O}i}(k+1)]^\mathrm{T}$ in (15), (8) can be discretized as follows:

$$x_i(k+1) = A_{\mathrm{d}i}x(k) + B_{\mathrm{d}i} \tag{16}$$

where

$$\begin{aligned}A_{\mathrm{d}i} &= e^{A_iT},\\ B_{\mathrm{d}i} &= \int_0^T e^{A_i(T-\tau)}B_i\mathrm{d}\tau = \left(\int_0^T e^{A_i(T-\tau)}\mathrm{d}\tau\right)B_i\\ &= A_i^{-1}(e^{A_iT}-I)B_i.\end{aligned}$$

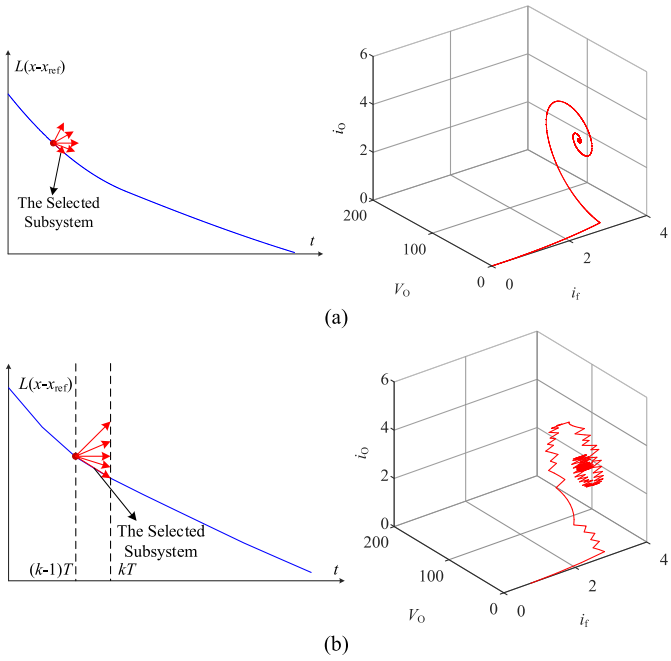

Fig. 2. Differences between the switched control in Theorem 1 and the discretized one. (a) Principle of the switched control in Theorem 1. (b) Principle of the switched control discretized in this article.

Therefore, (15) is the discretized expression of Theorem 1, and (16) can be used to predict the state variable in the next control period. It can be seen that the discretized switched control can be regarded as a special case of finite control set MPC, where (15) is the cost function with weight factors of L_f, C_f, and L_O. Moreover, the three weight factors are also the parameters of the energy storage components in the UETS.

The UETS shown in Fig. 1 can be used as an example to show the differences between the switched control in Theorem 1 and the discretized one. The initial state variable is set to $[0\ 0\ 0]^\mathrm{T}$, the reference state variable x_ref is set to $[3\ 49.5\ 3]^\mathrm{T}$. R_O and L_O are also set to 16.5 Ω and 4.39 mH, respectively. Thus, A and P can be calculated based on Table I. Fig. 2(a) shows the working principle of the switched control in Theorem 1. The derivatives of the Lyapunov function $L(x - x_\mathrm{ref})$ for all the subsystems are derived and ordered at every moment, so that the optimal subsystem is selected at any time. The system state trajectory will eventually converge to x_ref as fast as possible, and there will be no more movement or ripple.

Fig. 2(b) shows the working principle of the discretized switched control. The derivatives of the Lyapunov function $L(x - x_\mathrm{ref})$ for all the subsystems are only derived and ordered at the instant of kT. Thus, the selected subsystem is only optimal for the next control period. The system state trajectory will converge to x_ref slower and eventually move around x_ref in a limit cycle. The resonance in Fig. 2(b) means the small movement of the state trajectory.

In terms of control effect, the switched control described in Theorem 1 is better than the proposed DSCBOLF, because of the enough fast dynamic performance and the nonexistent ripple in Fig. 2(a). The proposed DSCBOLF for the UETS is discretized

from the switched control in Theorem 1, during which the control effect is traded off for a reduction of the required switching frequencies and computation, and the reduced switching frequencies and computation make the proposed DSCBOLF more suitable for industrial applications.

C. Computation Reduction for the DSCBOLF

The prediction in (16) and the optimization in (15) are required by the proposed DSCBOLF in each control period, which still costs many calculations. To further simplify the control algorithm, the Taylor expansion in the following is considered:

$$e^{AT} = I + AT + \frac{1}{2}A^2T^2 + \cdots + \frac{1}{m!}A^mT^m + \cdots = \sum_{k=0}^{\infty}\frac{1}{m!}A^mT^m. \quad (17)$$

Equation (17) can be approximated as (18) by neglecting the higher order terms of T. Since T is small enough, the higher terms in (17) are approximately equal to 0, so that the approximation in (18) is accurate enough and the system stability is not affected

$$e^{AT} \approx I + AT. \quad (18)$$

Therefore, $A_{\mathrm{d}i}$ and $B_{\mathrm{d}i}$ can be approximated as follows:

$$A_{\mathrm{d}i} \approx I + A_iT \quad (19)$$

$$B_{\mathrm{d}i} \approx B_iT. \quad (20)$$

Because of $B_i(2,0) = B_i(3,0) = 0$, $i_{\mathrm{f}i}(k+1)$, $V_{\mathrm{O}i}(k+1)$, and $i_{\mathrm{O}i}(k+1)$ can be calculated as (21)–(23), respectively

$$i_{\mathrm{f}i}(k+1) = \left(1 - \frac{r_{\mathrm{f}}T}{L_{\mathrm{f}}}\right) i_{\mathrm{f}}(k) - \frac{T}{L_{\mathrm{f}}}V_{\mathrm{O}}(k) + \frac{V_{\mathrm{dc}}T}{L_{\mathrm{f}}}(3-i) \quad (21)$$

$$V_{\mathrm{O}i}(k+1) = \frac{T}{C_{\mathrm{f}}}i_{\mathrm{f}}(k) - \frac{T}{C_{\mathrm{f}}}i_{\mathrm{O}}(k) \quad (22)$$

$$i_{\mathrm{O}i}(k+1) = \frac{T}{L_{\mathrm{O}}}V_{\mathrm{O}}(k) + \left(1 - \frac{R_{\mathrm{O}}T}{L_{\mathrm{O}}}\right) i_{\mathrm{O}}(k). \quad (23)$$

It can be seen that $V_{\mathrm{O}i}(k+1)$ and $i_{\mathrm{O}i}(k+1)$ will be invariable no matter which subsystem is selected. Thus, the optimization problem in (15) will be order reduced and simplified as follows:

$$\sigma(t) = \arg\min_{i\in K}\{L_{\mathrm{f}}(i_{\mathrm{f}i}(k+1) - i_{\mathrm{fref}}(k+1))^2\} = \arg\min_{i\in K}\{|i_{\mathrm{f}i}(k+1) - i_{\mathrm{fref}}(k+1)|\}. \quad (24)$$

It can also be seen from (21) that the relationship between $i_{\mathrm{f}i}$ and i is linear and monotonous, then the optimal solution of (24) must be the integer that makes $|i_{\mathrm{f}i}(k+1) - i_{\mathrm{fref}}(k+1)|$ nearest 0. Therefore, (24) can be solved by the following:

$$\sigma(t) = \mathrm{round}\left(i\,\big|_{i_{\mathrm{f}i}(k+1) - i_{\mathrm{fref}}(k+1) = 0}\right) = \mathrm{round}\left(\frac{L_{\mathrm{f}} - r_{\mathrm{f}}T}{V_{\mathrm{dc}}T}i_{\mathrm{f}}(k) - \frac{V_{\mathrm{O}}(k)}{V_{\mathrm{dc}}} - \frac{L_{\mathrm{f}}}{V_{\mathrm{dc}}T}i_{\mathrm{fref}}(k+1) + 3\right) \quad (25)$$

TABLE III
ACTION TIMES WHEN THE ADJACENT SUBSYSTEMS SWITCH WITH EACH OTHER

Switching Subsystems	Corresponding Switching State	Action Devices	Action Times
Subsystem 1 and Subsystem 2	S1 and S2	S_{b2} and S_{b4}	2
	S1 and S3	S_{a1} and S_{a3}	2
Subsystem 2 and Subsystem 3	S4 and S2	S_{b1} and S_{b3}	2
	S4 and S3	S_{a1}, S_{a3}, S_{b1}, S_{b2}, S_{b3}, S_{b4}	6
	S5 and S2	S_{a1} and S_{a3}	2
	S5 and S3	S_{b2} and S_{b4}	2
	S6 and S2	S_{a1}, S_{a2}, S_{a3}, S_{a4}, S_{b2}, S_{b4}	6
	S6 and S3	S_{a2} and S_{a4}	2
Subsystem 3 and Subsystem 4	S4 and S7	S_{a1} and S_{a3}	2
	S4 and S8	S_{a1}, S_{a2}, S_{a3}, S_{a4}, S_{b2}, S_{b4}	6
	S5 and S7	S_{b1} and S_{b3}	2
	S5 and S8	S_{a2} and S_{a4}	2
	S6 and S7	S_{a2}, S_{a4}, S_{b1}, S_{b2}, S_{b3}, S_{b4}	6
	S6 and S8	S_{b2} and S_{b4}	2
Subsystem 4 and Subsystem 5	S7 and S9	S_{a2} and S_{a4}	2
	S8 and S9	S_{b1} and S_{b3}	2

where *round*(x) is the rounding function equal to the integer nearest x, and $i_{\mathrm{fref}}(k+1)$ can be calculated using (26) and (27) as

$$V_{\mathrm{Oref}}(k+1) = R_{\mathrm{O}}i_{\mathrm{Oref}}(k) + L_{\mathrm{O}}\frac{i_{\mathrm{Oref}}(k+1) - i_{\mathrm{Oref}}(k)}{T} \quad (26)$$

$$i_{\mathrm{fref}}(k+1) = C_{\mathrm{f}}\frac{V_{\mathrm{Oref}}(k+1) - V_{\mathrm{Oref}}(k)}{T} + i_{\mathrm{Oref}}(k+1). \quad (27)$$

In this way, the computational burden of the proposed DSCBOLF can be greatly reduced.

D. Proposed Switching State Selection Method

Table II summarizes that there are multiple switching states to be selected when the full-bridge NPC inverter outputs levels of V_{dc}, 0, or $-V_{\mathrm{dc}}$, which makes the determination of the switching state complicated. Aiming at this problem, in [24], a quadratic term was added to the cost function to evaluate the switching action times, so that the cost function had to be calculated nine times for the nine switching states within each control period. Thus, more computation was required. In this article, a novel switching state selection method is proposed to cooperate with the proposed DSCBOLF, which can make the switching frequencies lower and consistent simultaneously, at the expense of little computation.

In steady state operation, the UETS is generally switched between adjacent subsystems. Fig. 3 and Table III shows the

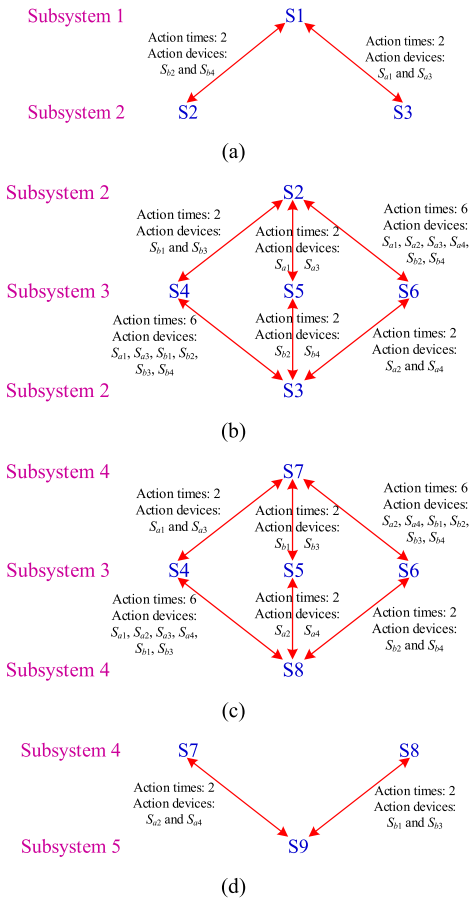

Fig. 3. Switching actions when the adjacent subsystems are switched with each other. (a) Switching between Subsystem 1 and Subsystem 2. (b) Switching between Subsystem 2 and Subsystem 3. (c) Switching between Subsystem 3 and Subsystem 4. (d) Switching between Subsystem 4 and Subsystem 5.

action devices and the switching action times when adjacent subsystems are switched with each other. It can be seen that up to six switches will be turned ON or OFF if the switching state is switched between S4 and S3, S6 and S2, S4 and S8, or S6 and S7. In order to minimize the switching frequencies, the cases of six switching actions are not allowed to appear. Thus, S5 has to be selected if the UETS is required to switch to Subsystem 3.

On this basis, in order to make the switching frequencies consistent, all switches must have the same action times. Then, if we want to make the action times of S_{b2} and S_{b4} the same as that of S_{a1} and S_{a3}, as shown in Fig. 3(a), S2 and S3 must be selected the same times. The same conclusion can be drawn from Fig. 3(b). Similarly, if we want to make the action times of S_{b1} and S_{b3} the same as that of S_{a2} and S_{a4}, as shown in Fig. 3(c) and (d), S7 and S8 must be selected the same times.

In addition, if the required waveform of the UETS is odd symmetric, the number of cases in Fig. 3(a) and (d) is the same, and the number of cases in Fig. 3(b) and (c) is also the same. Therefore, the switching frequencies of the eight switches will be all consistent, if S2, S3, S7, and S8 are all selected the same times.

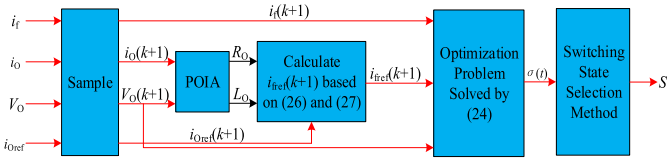

Fig. 4. Diagram of overall control flow of the parameter identification and Lyapunov function based adaptive control for the UETS.

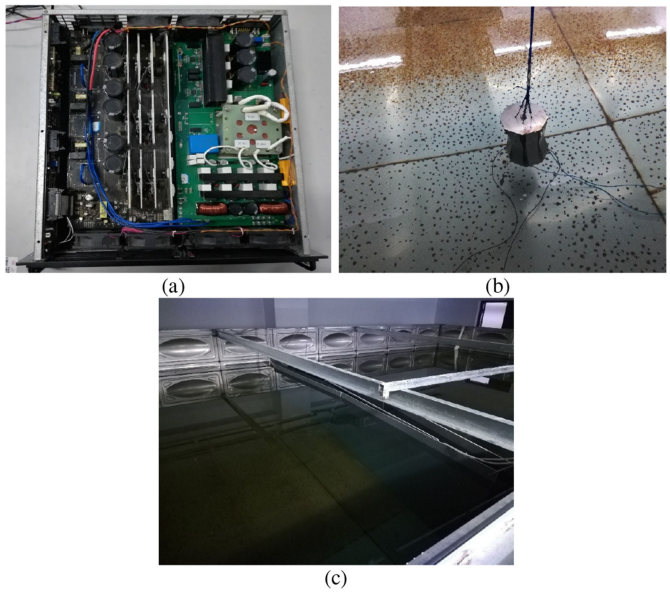

Fig. 5. Designed electroacoustic transduction platform. (a) Voltage mode amplifier. (b) Used GMT. (c) Acoustic pool.

Thus, the proposed switching state selection method can be expressed as follows. If $\sigma(t)$ obtained from (11) is equal to $\sigma(t\text{-}T)$, the value in the last control period, then S should remain unchanged. If $\sigma(t)$ is not equal to $\sigma(t\text{-}T)$, then the determination of S needs further discussion. If $\sigma(t) = 1$, $S =$ S1. If $\sigma(t) = 2$, S is selected alternately from S2 and S3. If $\sigma(t) = 3$, $S =$ S5. If $\sigma(t) = 4$, S is selected alternately from S7 and S8. If $\sigma(t) = 5$, $S =$ S9. Compared with the conventional phase shift modulation, the proposed switching state selection method does not require additional modulators and is easier to be implemented.

E. Overall Control Process

According to the analysis mentioned above, the overall control flow of the parameter identification and Lyapunov function based adaptive switched control for the UETS is shown in Fig. 4.

The first step is initialization. The control period T and the parameter identification period T_D should be given first. For the purpose of simplifying hardware and software design, T_D can be set to an integer multiple of T.

The second step is to sample the system state variables i_f, V_O, i_O and the output current reference i_{Oref} according to the control period T.

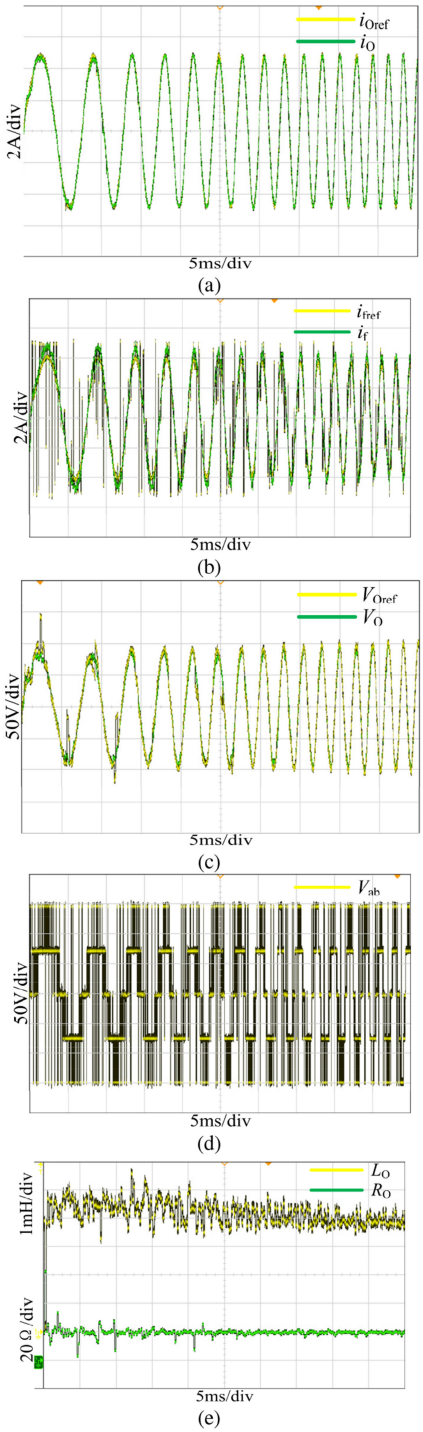

Fig. 6. Experiment results using the least square method. (a) Waveforms of i_{O} and i_{Oref}. (b) Waveforms of i_{f} and i_{fref}. (c) Waveforms of V_{O} and V_{Oref}. (d) Waveform of V_{ab}. (e) Identified R_{O} and L_{O}.

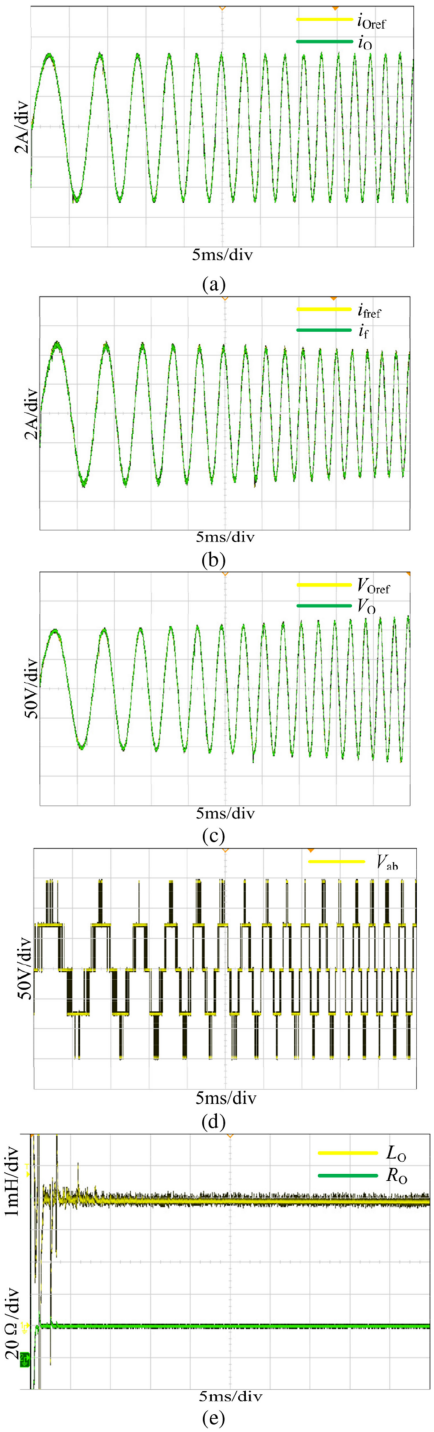

Fig. 7. Experiment results using the proposed POIA. (a) Waveforms of i_{O} and i_{Oref}. (b) Waveforms of i_{f} and i_{fref}. (c) Waveforms of V_{O} and V_{Oref}. (d) Waveform of V_{ab}. (e) Identified R_{O} and L_{O}.

In the third step, the equivalent parameters R_{O} and L_{O} of the GMT are identified by the proposed POIA.

The fourth step is to calculate the filter inductance current reference $i_{\mathrm{fref}}(k+1)$ based on (26) and (27).

The fifth step is to solve the optimization problem in (15) by (24).

The sixth step is to select the optimal switching state. If $\sigma(t)$ is equal to $\sigma(t\text{-}T)$, then S remains unchanged as it was in the last control period. Conversely, S is selected according to the proposed switching state selection method in D of Section IV.

V. Experiment Verification

To verify the feasibility and validity of the parameter identification and Lyapunov function based adaptive switched control,

TABLE IV
COMPARISON OF THE PROPOSED POIA AND THE LEAST SQUARE METHOD

Comparison Index	Least Square Method	Proposed POIA
Addition times	400	8
Subtraction times	154	3
Multiplicative times	256	10
Division times	5	10
FIFO units	150	6

a 1 kW electroacoustic transduction platform as shown in Fig. 5 was designed in the laboratory. The main circuit parameters are shown in Table I. The proposed DSCBOLF is realized in a Texas Instruments TMS320F28335 DSP. The parameter identification is realized in a XC95288XL CPLD. The sampling period and control period T is set to be 10 μs. Thus, the maximum switching frequency is 50 kHz. In fact, the designed voltage mode amplifier uses SGH80N60UFD type fast IGBTs and DSE130-60A type fast recovery diodes, whose maximum switching frequencies can be up to 100 kHz. The parameter identification period T_{D} is set to be 50 μs, and a dead time of 2 μs is added to the switching signals.

In order to verify the feasibility and validity of the proposed POIA, a 20 Ω resistor and a 10 mH inductor are connected in series as the load of the voltage mode amplifier. The output current reference i_{Oref} is set to be a linear chirp signal, whose amplitude is 4.24 and frequency is increased to 500 Hz from 100 Hz in 0.05 s. Combined with the proposed DSCBOLF, the proposed POIA is compared with the least square method. The first experiment employs the least square method where 50 sets of sampling data are used to identify the load online. Results of the first experiment are shown in Fig. 6, where (a) shows the waveforms of i_{O} and i_{Oref}, (b) shows the waveforms of i_{f} and i_{fref}, (c) shows the waveforms of V_{O} and V_{Oref}, (d) shows the waveforms of V_{ab}, and (e) shows the parameter identification results. The second experiment is carried out using the proposed POIA, and its results are shown in Fig. 7. At the same time, Table IV compares the memories and computations required by the two identification algorithms.

The comparison between Figs. 6 and 7 shows that the identification results of the least square method are not accurate enough, and the identification errors lead to large output fluctuation. But, the results of the proposed POIA are more accurate, which makes the output control effect greatly improved, and the validity of the proposed POIA is also proved when nonsinusoidal waves are required. In addition, Table IV shows that the computation and memory required by the POIA are much lower than the least square method.

In order to verify that the proposed adaptive switched control can improve system robustness and high precision control simultaneously, i_{Oref} is set as a 3 A sine wave whose frequency could be set to 100, 500, and 1000 Hz, respectively. Three groups of experiments are performed with the three frequencies. The first group results are shown in Fig. 8, where (a) shows the waveforms of i_{O} and i_{Oref}, (b) shows the waveforms of i_{f} and i_{fref}, (c) shows the waveforms of V_{O} and V_{Oref}, (d) shows the

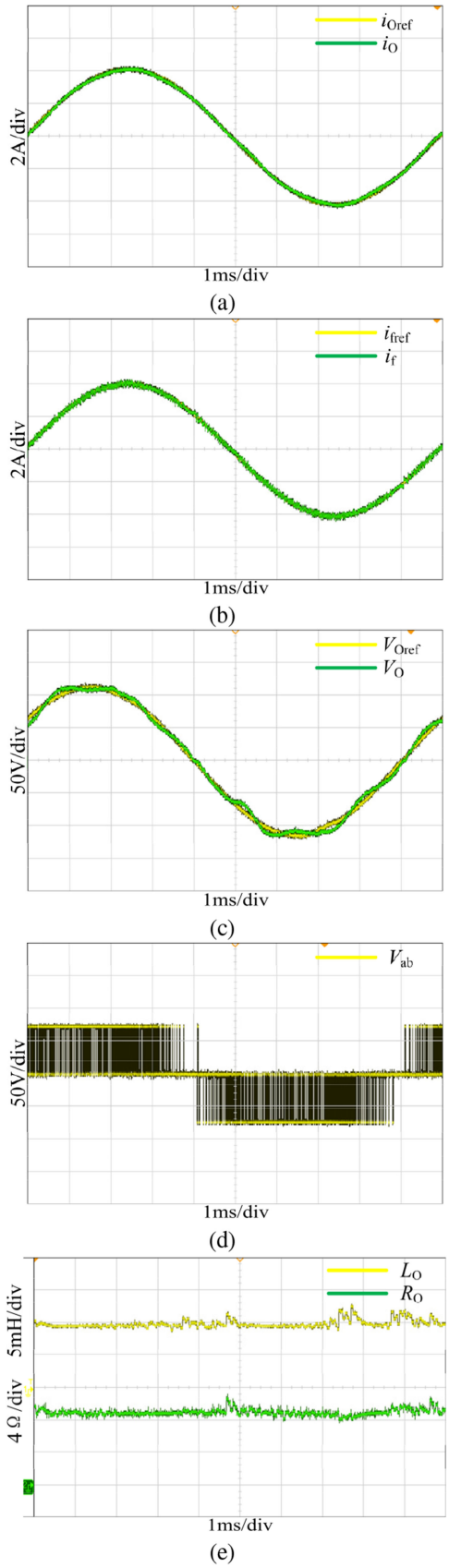

Fig. 8. Experiment results when $i_{\mathrm{Oref}} = 4.24\sin(628t)$. (a) Waveforms of i_{O} and i_{Oref}. (b) Waveforms of i_{f} and i_{fref}. (c) Waveforms of V_{O} and V_{Oref}. (d) Waveform of V_{ab}. (e) Identified R_{O} and L_{O}.

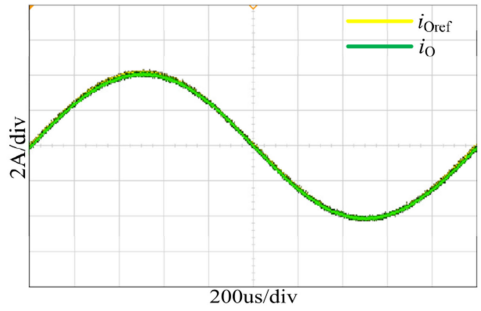

(a)

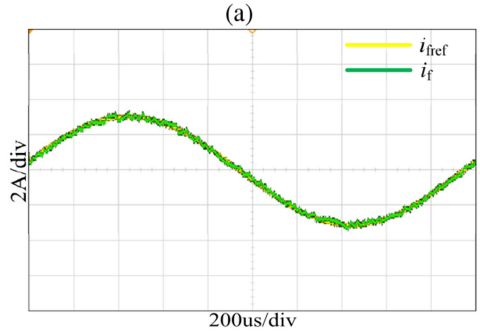

(b)

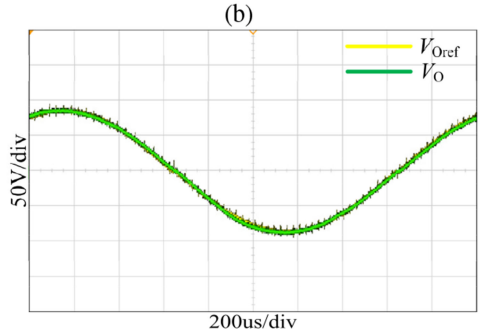

(c)

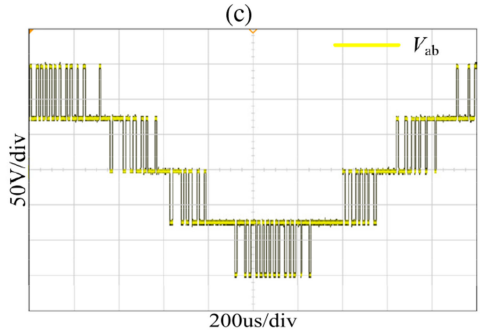

(d)

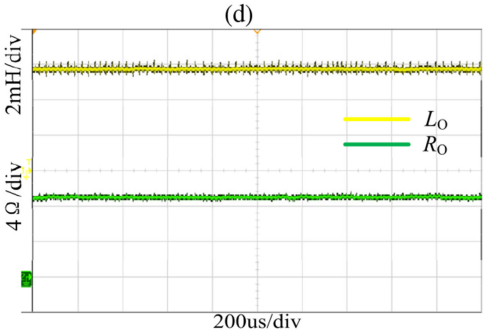

(e)

Fig. 9. Experiment results when $i_{\mathrm{Oref}} = 4.24\sin(3141t)$. (a) Waveforms of i_{O} and i_{Oref}. (b) Waveforms of i_{f} and i_{fref}. (c) Waveforms of V_{O} and V_{Oref}. (d) Waveform of V_{ab}. (e) Identified R_{O} and L_{O}.

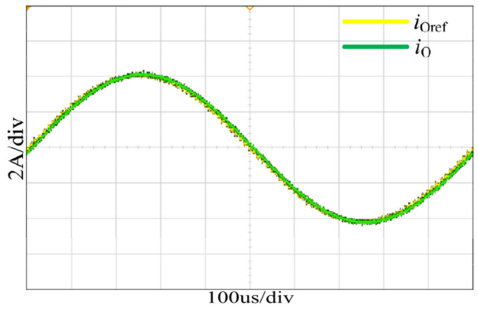

(a)

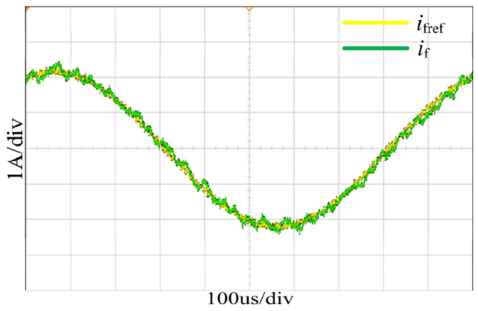

(b)

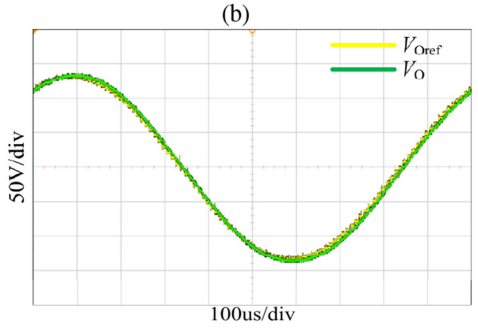

(c)

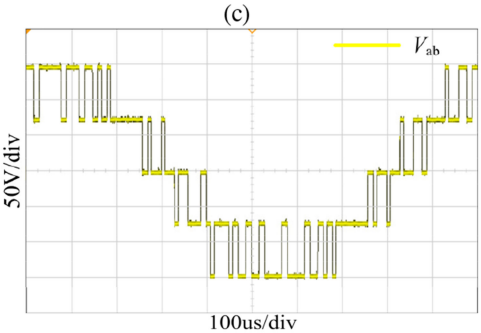

(d)

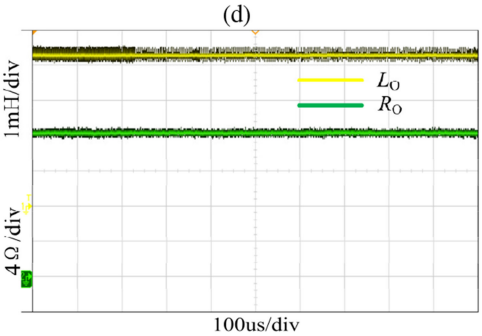

(e)

Fig. 10. Experiment results when $i_{\mathrm{Oref}} = 4.24\sin(6280t)$. (a) Waveforms of i_{O} and i_{Oref}. (b) Waveforms of i_{f} and i_{fref}. (c) Waveforms of V_{O} and V_{Oref}. (d) Waveform of V_{ab}. (e) Identified of R_{O} and L_{O}.

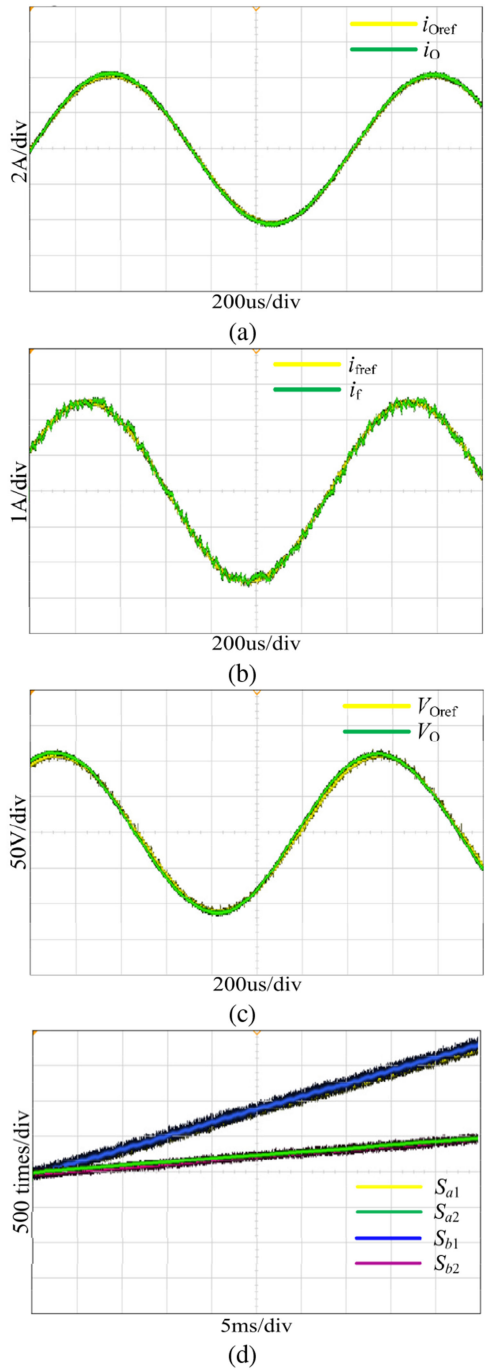

Fig. 11. Experiment results using the general MPC. (a) Waveforms of i_O and i_{Oref}. (b) Waveforms of i_f and i_{fref}. (c) Waveforms of V_O and V_{Oref}. (d) Waveforms of the cumulative pulse numbers of S_{a1}, S_{a2}, S_{b1}, and S_{b2}.

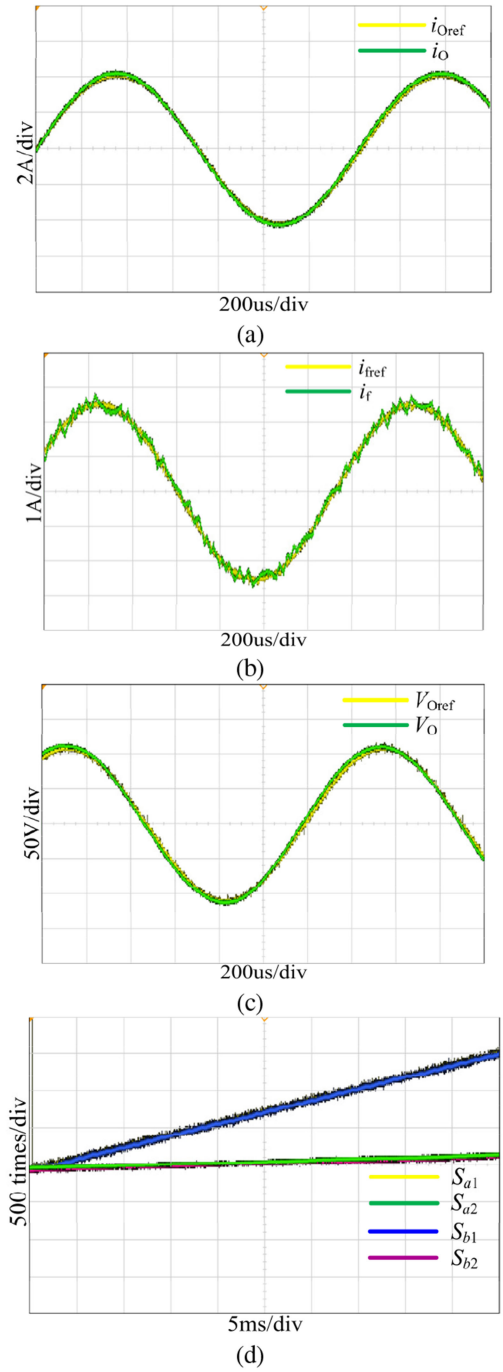

Fig. 12. Experiment results using the MPC in [24]. (a) Waveforms of i_O and i_{Oref}. (b) Waveforms of i_f and i_{fref}. (c) Waveforms of V_O and V_{Oref}. (d) Waveforms of the cumulative pulse numbers of S_{a1}, S_{a2}, S_{b1}, and S_{b2}.

waveform of V_{ab}, and (e) shows the waveforms of the R_O and L_O obtained by the proposed POIA. The experiment results of the second and third groups are shown in Figs. 9 and 10, respectively.

From the experiment results, it can be seen that i_{Oref} can be tracked quickly and accurately, and the system stability is ensured under different experiment conditions. In addition, the comparison of the three groups of experiments also shows that the equivalent inductance and resistance of the GMT vary greatly with its working frequency. However, the proposed DSCBOLF combined with the POIA successfully achieved adaptive control with acceptable control effect under different experiment conditions.

In order to verify that the proposed switching state selection method can make the switching frequencies lower and consistent with less computation, the general MPC without any switching state selection methods and the MPC in [24] are used to compare with the proposed DSCBOLF. In the experiment, i_{Oref} is set to

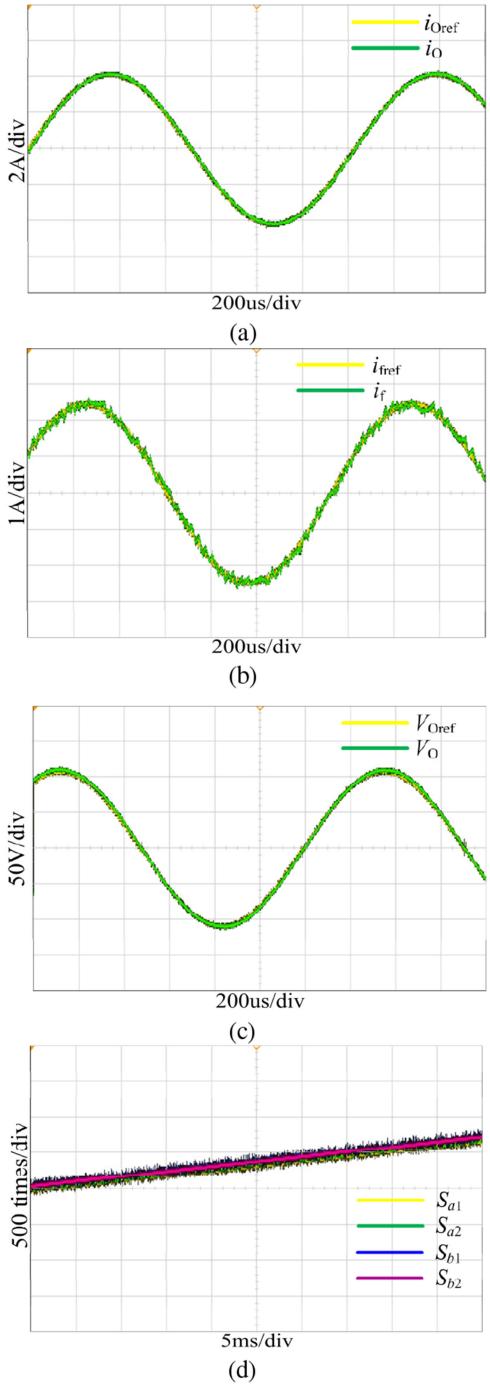

Fig. 13. Experiment results using the proposed DSCBOLF. (a) Waveforms of $i_{\rm O}$ and $i_{\rm Oref}$. (b) Waveforms of $i_{\rm f}$ and $i_{\rm fref}$. (c) Waveforms of $V_{\rm O}$ and $V_{\rm Oref}$. (d) Waveforms of the cumulative pulse numbers of S_{a1}, S_{a2}, S_{b1}, and S_{b2}.

a sine wave of 3 A and 700 Hz. The experiment results based on the general MPC are shown in Fig. 11, where (a) shows the waveforms of $i_{\rm O}$ and $i_{\rm Oref}$, (b) shows the waveforms of $i_{\rm f}$ and $i_{\rm fref}$, (c) shows the waveforms of $V_{\rm O}$ and $V_{\rm Oref}$, and (d) shows the waveforms of the cumulative pulse numbers of S_{a1}, S_{a2}, S_{b1}, and S_{b2}. The experiment results based on the MPC in [24] are shown in Fig. 12, and that based on the proposed DSCBOLF are shown in Fig. 13. Besides, Table IV shows the required computation and memory, the resulting average switching frequency,

TABLE V
COMPARISON OF MPC AND THE DSCBOLF

Comparison Index	General MPC	MPC in [24]	DSCBOLF in This Article
Addition times	27	81	1
Subtraction times	36	36	2
Multiplication times	72	90	3
FIFO units	0	4	1
Consistency	Inconsistent	Inconsistent	Consistent
Average switching frequency	11.61 kHz	8.81 kHz	6.79 kHz

the consistency of the switching frequencies of the three control methods.

From Table V and these experiment waveforms, it can be seen that the control effects of the three control methods are similar. However, if the general MPC is used, the resulting switching frequencies are higher and inconsistent with a large amount of calculation. The average switching frequency can be reduced using the MPC in [24], but the consistency still cannot be achieved, and the required computation and memory are the highest. In contrast, the proposed switching state selection method can not only greatly reduce the average switching frequency, but also achieve the consistency of the switching frequencies with the least computation.

VI. CONCLUSION

In this article, a parameter identification and Lyapunov function based adaptive switched control, consisting of a novel POIA and a DSCBOLF, is proposed for the UETS. In the proposed POIA, two difference equations are derived from the dynamic differential equation of the GMT, so that the POIA is allowed to maintain validity in arbitrary waveform system, and the POIA only needs one matrix inversion and one low-pass filtering for a 2-D matrix, which costs less computation and memory. Based on the parameters identified by the POIA, a DSCBOLF is derived, which can be realized in actual power electronic systems with acceptable switching frequencies and computation. In addition, a novel switching state selection method is also proposed to cooperate with the DSCBOLF, which makes the switching frequencies lower and consistent simultaneously with less computation. Therefore, based on the proposed POIA and DSCBOLF, the parameter identification and Lyapunov function based adaptive switched control can greatly improve system robustness against the parameter variations of the GMT in arbitrary waveform system. Finally, the experiment results demonstrate the feasibility and validity of the proposed method.

REFERENCES

[1] A. K. Morozov *et al.*, "High-efficient tunable sound sources for ocean and bottom tomography, 15 years of operating history," in *Proc. IEEE OCEANS*, Monterey, CA, USA, 2016, pp. 1–10.
[2] A. K. Morozov, "Tunable and broadband resonator pipe sound sources for ocean acoustic tomography, communications and long-range navigation," in *Proc. IEEE OCEANS*, Aberdeen, U.K., 2017, pp. 1–8.

[3] T. C. Montgomery, R. J. Meyer, and E. M. Bienert, "Broadband transduction implementation and system impact," in *Proc. IEEE OCEANS*, Vancouver, WA, USA, 2007, pp. 1–5.
[4] L. Freitag, P. Koski, A. K. Morozov, S. Singh, and J. Partan, "Acoustic communications and navigation under Arctic ice," in *Proc. IEEE OCEANS*, Hampton Roads, VA, USA, 2012, pp. 1–8.
[5] L. Freitag and A. K. Morozov, Under-ice acoustic communications and navigation for gliders and AUVs, American Geophysical Union, in *Proc. Fall Meet.*, 2009, p. OS43B-1389.
[6] A. K. Morozov, K. F. Scussel, M. Wolf, and M. J. Coryer, "The new development of the autonomous sources for ocean acoustic navigation, tomography and communications," in *Proc. IEEE OCEANS*, Anchorage, AK, USA, 2017, pp. 1–8.
[7] K. Agbossou, J.-L. Dion, S. Carignan, M. Abdelkrim, and A. Cheriti, "Class D amplifier for a power piezoelectric load," *IEEE Trans. Ultrason., Ferroelect., Freq. Control*, vol. 47, no. 4, pp. 1036–1041, Jul. 2000.
[8] D. Nielsen, A. Knott, and M. A. E. Andersen, "A high-voltage class D audio amplifier for dielectric elastomer transducers," in *Proc. IEEE Appl. Power Electron. Conf. Expo.*, Fort Worth, TX, USA, 2014, pp. 3278–3283.
[9] S. Hu, S. Zhu, M. Zhong, and Q. He, "Neural network modeling and generalized predictive control for giant magnetostrictive actuators," in *Proc. Chinese Control Decis. Conf.*, Guilin, China, 2009, pp. 2981–2985.
[10] F. T. Calkins, R. C. Smith, and A. B. Flatau, "Energy-based hysteresis model for magnetostrictive transducers," *IEEE Trans. Magn.*, vol. 36, no. 2, pp. 429–439, Mar. 2000.
[11] D. L. Hall, "Dynamics and vibrations of magnetostrictive transducers," Ph.D. dissertation, Dept. Aerosp. Eng. Eng. Mech., Iowa State Univ., Ames, IA, USA, 1994.
[12] A. Vidal *et al.*, "A method for identification of the equivalent inductance and resistance in the plant model of current-controlled grid-tied converters," *IEEE Trans. Power Electron.*, vol. 30, no. 12, pp. 7245–7261, Dec. 2015.
[13] H. Akagi, S. Inoue, and T. Yoshii, "Control and performance of a transformerless cascade PWM STATCOM with star configuration," *IEEE Trans. Ind. Appl.*, vol. 43, no. 4, pp. 1041–1049, Jul./Aug. 2007.
[14] M. Konghirun and L. Xu, "A fast transient-current control strategy in sensorless vector-controlled permanent magnet synchronous motor," *IEEE Trans. Power Electron.*, vol. 21, no. 5, pp. 1508–1512, Sep. 2006.
[15] M. Hagiwara, R. Maeda, and H. Akagi, "Negative-sequence reactive-power control by a PWM STATCOM based on a modular multilevel cascade converter (MMCC-SDBC)," *IEEE Trans. Ind. Appl.*, vol. 48, no. 2, pp. 720–729, Mar./Apr. 2012.
[16] H. Ertl, J. W. Kolar, and F. C. Zach, "Analysis of a multilevel multicell switch-mode power amplifier employing the "flying-battery" concept," *IEEE Trans. Ind. Electron.*, vol. 49, no. 4, pp. 816–823, Aug. 2002.
[17] M. Dong, Y. Zhang, M. Xia. and J. Li, "Multilevel dual closed-loop controlling class-D power amplifier with FPGA," in *Proc. Int. Conf. Control Eng. Commun. Technol.*, Liaoning, China, 2012, pp. 421–425.
[18] J. Zhou, Z. Deng, C. Liu, K. Li, and J. He, "Current ripple analysis of five-phase six-leg switching power amplifiers for magnetic bearing with one-cycle control," in *Proc. 19th Int. Conf. Electr. Mach. Syst.*, Chiba, Japan, 2016, pp. 1–6.
[19] S. Yu and M. Tseng, "Optimal control of a nine-level class-D audio amplifier using sliding-mode quantization," *IEEE Trans. Ind. Electron.*, vol. 58, no. 7, pp. 3069–3076, Jul. 2011.
[20] Y. Zhang, Q. Meng, Y. Li, and L. Cai, "A high-efficiency cascaded multilevel class-D amplifier with FPGA based on sliding mode control," in *Proc. Int. Symp. Syst. Control Aeronautics/Astronautics*, Harbin, China, 2010, pp. 86–90.
[21] J. Fang and Y. Ren, "Self-adaptive phase-lead compensation based on unsymmetrical current sampling resistance network for magnetic bearing switching power amplifiers," *IEEE Trans. Ind. Electron.*, vol. 59, no. 2, pp. 1218–1227, Feb. 2012.
[22] L. Tarisciotti, P. Zanchetta, A. Watson, J. Clare, and S. Bifaretti, "A comparison between dead-beat and predictive control for a 7-level back-to-back cascaded H-bridge under fault conditions," in *Proc. IEEE ECCE*, 2013, pp. 2147–2154.
[23] S. Vazquez *et al.*, "Model predictive control for single-phase NPC converters based on optimal switching sequences," *IEEE Trans. Ind. Electron.*, vol. 63, no. 12, pp. 7533–7541, Dec. 2016.
[24] P. Stolze, M. Kramkowski, T. Mouton, M. Tomlinson, and R. Kennel, "Increasing the performance of finite-set model predictive control by oversampling," in *Proc. IEEE Int. Conf. Ind. Technol.*, Cape Town, South Africa, 2013, pp. 551–556.
[25] M. M. Peretz and S. Ben-Yaakov, "Time-domain identification of pulse-width modulated converters," *IET Power Electron.*, vol. 5, no. 2, pp. 166–172, Feb. 2012.
[26] R. Dutta and M. F. Rahman, "A comparative analysis of two test methods of measuring *d*- and *q*-axes inductances of interior permanent-magnet machine," *IEEE Trans. Magn.*, vol. 42, no. 11, pp. 3712–3718, Nov. 2006.
[27] A. Stankovic, E. R. Benedict, V. John, and T. A. Lipo, "A novel method for measuring induction machine magnetizing inductance," in *Proc. IEEE IAS Annu. Meet.*, New Orleans, LA, USA, 1997, pp. 234–238.
[28] Z. Hu and Y. Chen, "New method of live line measuring the inductance parameters of transmission lines based on GPS technology," *IEEE Trans. Power Del.*, vol. 23, no. 3, pp. 1288–1295, Jul. 2008.
[29] Y. Fan, L. Zhang, M. Cheng, and K. T. Chau, "Sensorless SVPWM-FADTC of a new flux-modulated permanent-magnet wheel motor based on a wide-speed sliding mode observer," *IEEE Trans. Ind. Electron.*, vol. 62, no. 5, pp. 3143–3151, May 2015.
[30] P. Cortes, G. Ortiz, J. I. Yuz, J. Rodriguez, S. Vazquez, and L. G. Franquelo, "Model predictive control of an inverter with output LC filter for UPS applications," *IEEE Trans. Ind. Electron.*, vol. 56, no. 6, pp. 1875–1883, Jun. 2009.
[31] L. Asiminoaei, R. Teodorescu, F. Blaabjerg, and U. Borup, "Implementation and test of an online embedded grid impedance estimation technique for PV inverters," *IEEE Trans. Ind. Electron.*, vol. 52, no. 4, pp. 1136–1144, Aug. 2005.
[32] A. Riccobono, M. Mirz, and A. Monti, "Noninvasive online parametric identification of three-phase AC power impedances to assess the stability of grid-tied power electronic inverters in LV networks," *IEEE J. Emerg. Sel. Top. Power Electron.*, vol. 6, no. 2, pp. 629–647, Jun. 2018.
[33] P. García, M. Sumner, Á. Navarro-Rodríguez, J. M. Guerrero, and J. García, "Observer-based pulsed signal injection for grid impedance estimation in three-phase systems," *IEEE Trans. Ind. Electron.*, vol. 65, no. 10, pp. 7888–7899, Oct. 2018.
[34] C. H. Sherman and J. L. Butler, *Transducers and Arrays for Underwater Sound*. New York, NY, USA: Springer, 2007.
[35] J. M. Sewell and P M. Kuhn, "Opportunities and challenges in the use of Terfenol for sonar transducers," in *Power Sonic and Ultrasonic Transducers Design*. Berlin, Germany: Springer, 1988.
[36] S. H. Cho, H. J. Kim, and Y. Y. Kim, "Feasibility study of a membrane-type magnetostrictive acoustic transducer for ultrasonic thrombolysis," in *Proc. IEEE Int. Ultrasonics Symp.*, Rome, Italy, 2009, pp. 2225–2227.
[37] D. Satpathi, J. A. Moore, and M. G. Ennis, "Terfenol-D based optical current transducer," in *Proc. SENSORS, IEEE*, Toronto, Canada, 2003, pp. 403–408.
[38] M. Sheykholeslami, Y. Hojjat, M. Ghodsi, K. Kakavand, and S. Cinquemani, "Investigation of ΔE effect on vibrational behavior of giant magnetostrictive transducers," *Shock Vibration*, vol. 2015, pp. 1–9, 2015.
[39] G. S. Deaecto, J. C. Geromel, F. S. Garcia, and J. A. Pomilio, "Switched affine systems control design with application to DC-DC converters," *IET Control Theory Appl.*, vol. 4, no. 7, pp. 1201–1210, Jul. 2010.
[40] R. Gavagsaz-Ghoachani, M. Phattanasak, J. Martin, S. Pierfederici, B. Nahid-Mobarakeh, and P. Riedinger, "A Lyapunov function for switching command of a DC–DC power converter with an LC input filter," *IEEE Trans. Ind. Appl.*, vol. 53, no. 5, pp. 5041–5050, Sep./Oct. 2017.
[41] H. Sira-Ramirez, R. Ortega, and G. Escobar, "Lagrangian modeling of switch regulated DC-to-DC power converters," in *Proc. 35th IEEE Conf. Decis. Control*, Kobe, Japan, 1996, pp. 4492–4497.
[42] G. Escobar, A. J. V. D. Schaft, and R. Ortega, "A Hamiltonian viewpoint in the modeling of switching power converters," *Automatica*, vol. 35, no. 3, pp. 445–452, 1999.

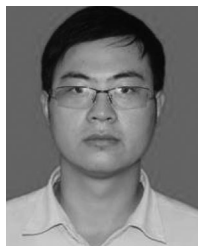

Xinwei Wei was born in Henan, China, 1990. He received the B.S. degree in electrical engineering and automation from Henan Normal University, Xinxiang, China, in 2014, and the M.S. degree from the College of Information Science and Engineering, Changsha University of Science & Technology, Changsha, China, in 2017. He is currently working toward the Ph.D. degree with the College of Electrical and Information Engineering, Hunan University, Changsha, China.

His research interests include power amplifiers, modular multilevel converters, reactive power compensation, model predictive control, and hybrid system.

Hongliang Wang (M'12–SM'15) received the B.Sc. degree in electrical engineering from the Anhui University of Science and Technology, Huainan, China, in 2004, and the Ph.D. degree in electrical engineering from the Huazhong University of Science and Technology, Wuhan, China, in 2011.

From 2004 to 2005, he was an Electrical Engineer with Zhejiang Hengdian Thermal Power Plant. From 2011 to 2013, he was a Senior System Engineer with Sungrow Power Supply Co., Ltd. From 2013 to 2018, he was a Postdoctoral Fellow with Queen's University. Since 2018, he has been with Hunan University, Changsha, China, where he is currently a Full Professor with the College of Electrical and Information Engineering. He has authored more than 60 technical papers in the journals and conferences. He is the inventor/co-inventor of 42 China issued patents, 8 U.S. issued patents. His research interests include multilevel topology, high-gain topology, parallel technology, and virtual synchronous generator technology for photovoltaic application and micro-grids application; resonant converters and server power supplies, and LED drivers.

Dr. Wang is currently a Senior Member of China Electro-Technical Society and a Senior Member of China Power Supply Society (CPSS). He is also a member of CPSS Technical Committee on Standardization; a member of CPSS Technical Committee on Renewable Energy Power Conversion, a China Expert Group Member of IEC Standard TC8/PT 62786, a Vice-Chair of IEEE Kingston Section, a Session Chair of ECCE 2015 and ECCE2017, a TPC member of ICEMS2012.

An Luo (SM'09) was born in Changsha, China, in 1957. He received the B.S. and M.S. degrees in industrial automation from Hunan University, Changsha, China, in 1982 and 1986, respectively, and the Ph.D. degree in fluid power transmission and control from Zhejiang University, Hangzhou, China, in 1993.

Between 1996 and 2002, he was a Professor with Central South University. Since 2003, he has been a Professor with the College of Electrical and Information Engineering, Hunan University, where he is also the Chief of National Electric Power Conversion and Control Engineering Technology Research Center. His research interests include distributed generation, microgrid, and power quality.

Dr. Luo was elected to the Chinese National Academy of Engineering in 2015, the highest honor for scientists and engineers and scientists in China. He has won the highly prestigious China National Science and Technology Awards three times (2014, 2010, and 2006).

Fujun Ma (M'15) was born in Hunan, China, 1985. He received the B.S. degree in automation and the Ph.D. degree in electrical engineering from Hunan University, Changsha, China, in 2008 and 2015, respectively.

Since 2013, he has been an Associate Professor with the College of Electrical and Information Engineering, Hunan University. His research interests include power quality managing technique of electrified railway, electric power saving, reactive power compensation, and active power filters.

Zhen Zhu was born in Hunan, China, 1988. He received the B.S. and M.S. degrees in automation from the College of Geophysics and Information Engineering, China University of Petroleum, Beijing, China, in 2013 and 2017, respectively. Since 2017, he has been working toward the Ph.D. degree in electrical engineering with the College of Electrical and Information Engineering, Hunan University, Changsha, China. His research interests include hybrid compensation of traction system and energy management of energy router.

Gaoxiang Li was born in Henan, China, 1990. He received the B.S. degree from the School of Electrical Engineering and Automation, Henan Polytechnic University, Jiaozuo, China, in 2014, and the M.S. degree from the College of Information Science and Engineering, Central South University, Changsha, China, in 2017. He is currently working toward the Ph.D. degree with the College of Electrical and Information Engineering, Hunan University, Changsha, China.

His research interests include power quality control, new energy generation, and subsynchronous oscillation suppression.

Renyifan Hao was born in Hunan, China, 1994. He received the B.S. and M.S. degrees in electrical engineering and automation from Hunan University, Changsha, in 2016 and 2019, respectively.

He is currently a Hardware Engineer with ZTE Corporation. His research interests include reactive power compensation, multilevel converter application technology, etc.